



UNIVERSITÀ DI PISA



Commissioning of the Mu2e tracker DAQ, planning for the Vertical Slice Test and pre-pattern recognition studies

Candidate:

Sara Gamba

Supervisors:

Pavel Murat (FNAL)

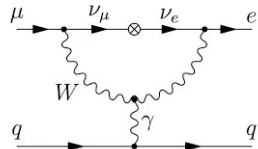
Simone Donati (Unipi, INFN Pisa)

October 21st 2024

Charged Lepton Flavour Violation

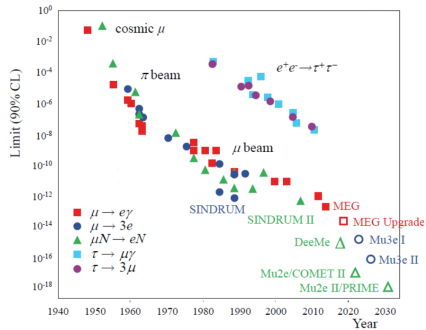
- The **Standard Model** (SM) does not predict lepton flavour violation;
- The discovery of **neutrino oscillations** proves that lepton interactions are non-diagonal in flavour;
- The SM fails to explain phenomena like neutrino masses and the consequent flavour oscillations;
- The branching ratios of **CLFV** processes, including neutrino oscillations, are suppressed by factors proportional to $(\Delta m_\nu^2)^2/M_W^4$ and expected to be less than $\mathcal{O}(10^{-50})$;
- This value is far beyond current experimental capabilities.

QUARKS		
mass $=2.2 \text{ MeV}/c^2$	$\frac{2}{3}$	$\frac{2}{3}$
charge $\frac{2}{3}$	$\frac{1}{2}$	$\frac{1}{2}$
spin $\frac{1}{2}$	u	c
	up	charm
mass $=4.7 \text{ MeV}/c^2$	-1	-1
charge $-1/3$	$\frac{1}{2}$	$\frac{1}{2}$
spin $\frac{1}{2}$	d	s
	down	strange
mass $=173.1 \text{ GeV}/c^2$	$\frac{2}{3}$	$\frac{2}{3}$
charge $\frac{2}{3}$	$\frac{1}{2}$	$\frac{1}{2}$
spin $\frac{1}{2}$	t	b
	top	bottom
LEPTONS		
mass $=0.511 \text{ MeV}/c^2$	-1	-1
charge -1	$\frac{1}{2}$	$\frac{1}{2}$
spin $\frac{1}{2}$	e	μ
	electron	muon
mass $=1.7768 \text{ GeV}/c^2$	-1	-1
charge -1	$\frac{1}{2}$	$\frac{1}{2}$
spin $\frac{1}{2}$	τ	tau
mass $<1.0 \text{ eV}/c^2$	0	0
charge 0	$\frac{1}{2}$	$\frac{1}{2}$
spin $\frac{1}{2}$	ν_e	ν_μ
mass $<0.17 \text{ MeV}/c^2$	0	0
charge 0	$\frac{1}{2}$	$\frac{1}{2}$
spin $\frac{1}{2}$	ν_τ	ν_τ
mass $<18.2 \text{ MeV}/c^2$	0	0
charge 0	$\frac{1}{2}$	$\frac{1}{2}$
spin $\frac{1}{2}$		
mass $<18.2 \text{ MeV}/c^2$	0	0
charge 0	$\frac{1}{2}$	$\frac{1}{2}$
spin $\frac{1}{2}$		



Search for CLFV

- ▶ New Physics (NP) models predict much higher rates of CLFV;
- ▶ Observing CLFV would provide unambiguous evidence of physics beyond the SM;
- ▶ CLFV channels involving muons:
 $\mu^+ \rightarrow e^+ \gamma$, $\mu^- N \rightarrow e^- N$ and
 $\mu^+ \rightarrow e^+ e^+ e^-$;
- ▶ $\mu^- N \rightarrow e^- N$ channel:
 - Higher momentum signal and better separation from the background;
 - Benefits from high intensity beam;
 - Better sensitivity to CLFV in a large range of NP scenarios.
- ▶ Current best limit on $\mu^- N \rightarrow e^- N$ by SINDRUM II: $R_{\mu e} < 7 \times 10^{-13}$ (90% CL).



The Mu2e experiment

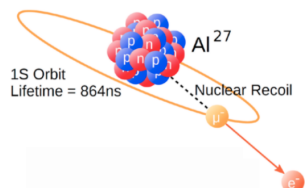
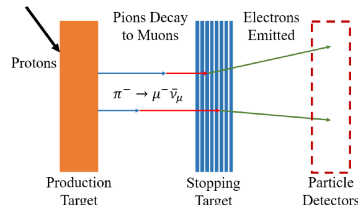
- ▶ Search for neutrinoless, coherent conversion $\mu^- N \rightarrow e^- N$ in the field of an Al nucleus, by measuring:

$$R_{\mu e} = \frac{\mu^- + N(Z, A) \rightarrow e^- + N(Z, A)}{\mu^- + N(Z, A) \rightarrow \nu_\mu + N(Z - 1, A)}$$

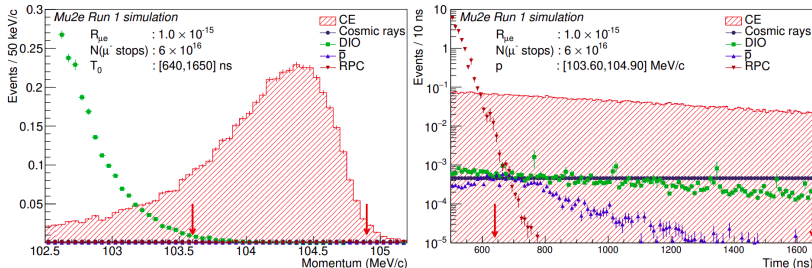
- ▶ Mu2e goal is to improve SINDRUM II limit by 4 orders of magnitude;
- ▶ The signal is a monochromatic conversion electron (CE) with energy:

$$E_{CE} = m_\mu - E_{recoil} - E_{bind} = 104.97 \text{ MeV}$$

where m_μ is the muon mass, E_{recoil} the target nucleus recoil energy and E_{bind} the muonic atom $1s$ state binding energy.

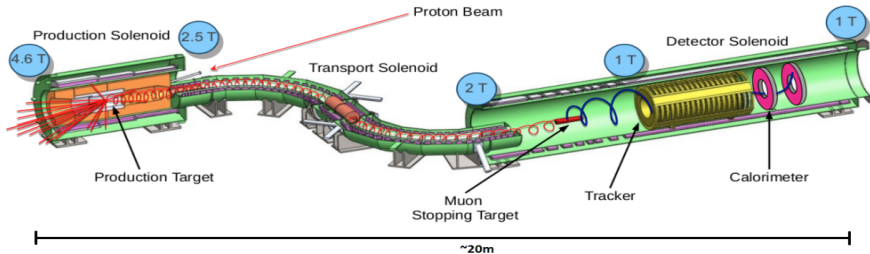


Background sources



- ▶ **Cosmics** → veto enclosing the detector (≈ 0.046 evs/RunI);
- ▶ **Intrinsic** → 1 MeV/c momentum resolution:
 - Decay In Orbit $\mu^- N \rightarrow e^- \bar{\nu}_e \nu_\mu N$ (≈ 0.038 evs/RunI);
 - Radiative Muon Capture $\mu^- N \rightarrow \gamma \nu_\mu N'^*$ (< 0.0024 evs/RunI).
- ▶ **Delayed processes from $\bar{p} \rightarrow$** absorbers in the TS (≈ 0.010 evs/RunI);
- ▶ **Prompt processes** → pulsed beam + delayed live window:
 - Radiative Pion Capture $\pi^- N \rightarrow \gamma N'^*$ (≈ 0.010 evs/RunI);
 - π and μ Decay In Flight ($< 2 \times 10^{-3}$ evs/RunI);
 - Beam electrons ($< 1 \times 10^{-3}$ evs/RunI).

The Mu2e experimental setup



► Production Solenoid:

- 8 GeV pulsed proton beam interacts with the W target and mostly π s are produced;
- graded field for backward collection.

► Transport Solenoid:

- it allows for π decay and μ transport;
- S-shape for charged particle selection;
- it selects muons with $p \lesssim 100$ MeV/c;
- rotating collimator COL3 selects μ^- or μ^+ beam.

► Detector Solenoid: Stopping Target, p absorber and detectors.

The electromagnetic calorimeter

Calorimeter is vital for:

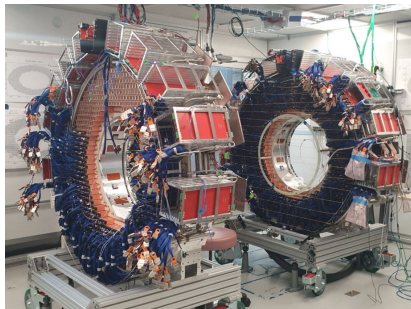
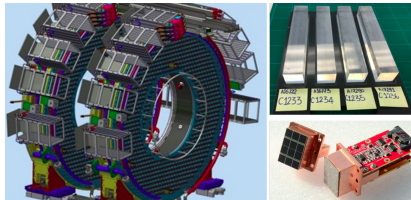
- ▶ **PID (E/p);**
- ▶ Seed for **track reconstruction;**
- ▶ Fast online **trigger filter.**

Design:

- ▶ 2 hollow disks of crystals, 70 cm apart;
- ▶ 2×674 CsI crystals per disk, each coupled to 2 SiPMs.

Performance:

- ▶ $\sigma_E/E \sim 10\%$;
- ▶ $\sigma_{xy} \sim 6$ mm;
- ▶ $\Delta t < 500$ ps.



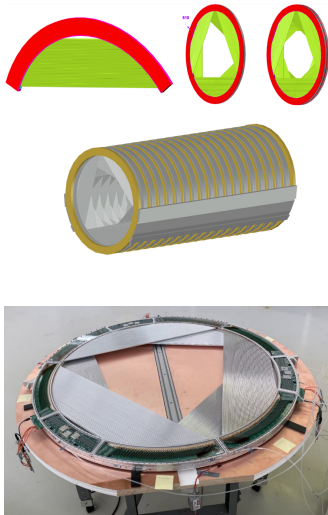
The straw tracker

Purpose:

- ▶ momentum measurement with $\Delta p < 300 \text{ keV}/c \text{ FWHM} + 950 \text{ keV}/c$ energy losses (ST and proton absorber).

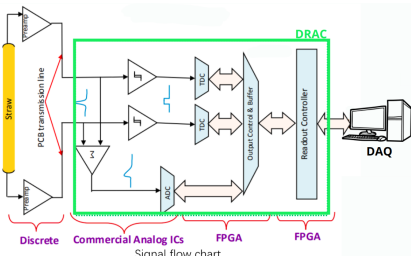
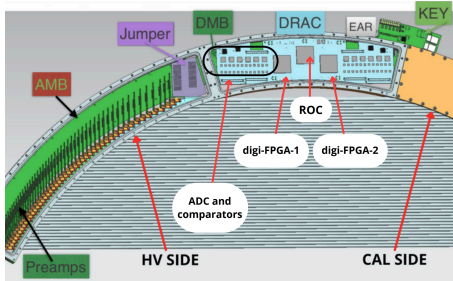
Design:

- ▶ 3 m downstream of the ST ($B \sim 1 \text{ T}$);
- ▶ hollow geometry (low p_T particles);
- ▶ 3 m long tracker in vacuum;
- ▶ 96 straws per panel, 6 panels per plane, 2 planes per station;
- ▶ 18 tracking stations: 216 panels;
- ▶ 5 mm diameter and 40-110 cm long straws filled with a 80%:20% Ar:CO₂ mixture at a pressure of 1 atm.



The tracker readout and DAQ

- ▶ Signal is readout from both ends by preamps;
- ▶ Analog signals are sent to the DRAC and processed by 2 TDCs and one ADC;
- ▶ The 2 digi-FPGA create one data packet for each hit with **two hit times** and **one waveform**;
- ▶ Data packets sent to ROC;
- ▶ ROC collects, buffers and transfers data from digi-FPGAs to DTC installed on DAQ computers;
- ▶ DTC sends data request to the ROC and sends data packet to the Event Builder.



My Thesis

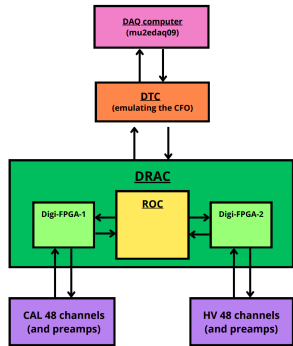
- ▶ Mu2e is starting detector **commissioning** and **calibration**;
- ▶ My work consists of a **comprehensive study of the Mu2e tracker**:
 - **Vertical Slice Test (VST)**. The entire testing chain, from the straws to the readout, to processed data on disk:
 - ▶ initial tracker **DAQ** and **FEE** testing.
 - First steps towards the tracker timing **calibration** with **cosmics**:
 - ▶ development of a **cosmic track reconstruction** procedure.
 - **Mu2e Offline**. Pre-pattern recognition studies:
 - ▶ estimated data volume for Mu2e data-taking is **>7 PB/year**;
 - ▶ the **primary source** of hits in the Mu2e tracker will be δ -electrons;
 - ▶ important to identify those hits without losing **CE efficiency**.

Outline

- ▶ Commissioning of the tracker DAQ and FEE:
 - validation of ROC readout;
 - study of preamplifiers performance.
- ▶ First steps towards the station calibration;
- ▶ Pre-pattern recognition studies;
- ▶ Conclusions.

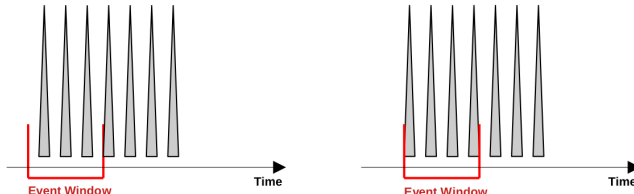
Description of test stand setup

- ▶ ROC readout validation;
- ▶ TS1 tracker test stand: one ROC (one tracker panel-96 channels), one DTC connected to the DAQ computer;
- ▶ Two different ROC data readout modes:
 - MODE 1: emulated data readout mode;
 - MODE 2: digi-FPGA readout mode.
- ▶ digi-FPGAs pulsed by their **internal pulser** at $f_{gen} = 250 \text{ kHz}$ or 60 kHz ;
- ▶ **Event Window (T_{EW})**: the time interval between two proton pulses, varied between 700 ns to $50 \mu\text{s}$;
- ▶ The ROC firmware has an internal **hit buffer** which stores up to **255 hits**.



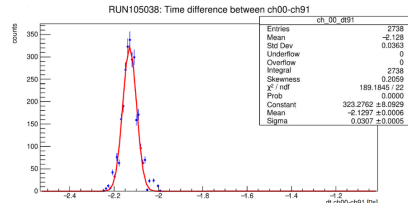
Logic of data taking

- ▶ Depending on $T_{gen} = 1/f_{gen}$ and T_{EW} , the data taking can proceed in two different modes:
 - $N_{gen} \geq 255$: $N_{readout} = 255$ (**overflow mode**);
 - $N_{gen} < 255$: $N_{readout} < 255$ (**underflow mode**);
- ▶ Each FPGA has its own generator and pulses from different generators are offset ($\in [0, T_{gen}]$) with respect to each other;
- ▶ Offsets between channels (same digi-FPGA) are about few ns and can be measured;
- ▶ Timing of generator pulses uncorrelated with the beginning of the EW
→ different number of hits in an EW;
- ▶ Channel readout sequence is fixed.



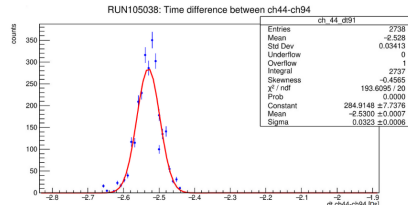
Monte Carlo simulation

- ROC readout logic emulated with a bit-level C++ simulation;
- Simulated parameters:
 - number of hits in each channel;
 - number of readout hits per event.
- digi-FPGAs and channel to channel offsets considered.

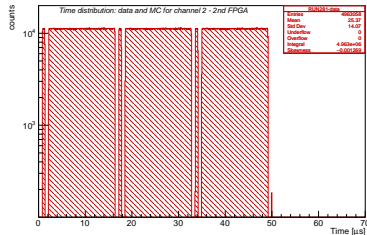
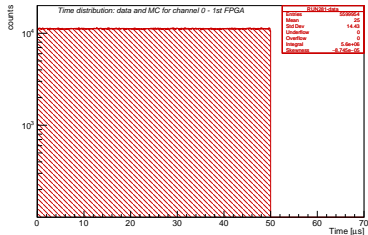


Steps of the simulation:

- EW starts at $t = 0$ s;
- The 1st pulse is generated $T_0 \in [0, T_{gen}]$;
- Next pulses: $T_i = T_{i-1} + T_{gen}$, until $T_i > T_{EW}$;
- Pulses are generated in each channel following the readout sequence;
- The procedure *continues* until all hits have been *readout*, or $N_{hits} > 255$.



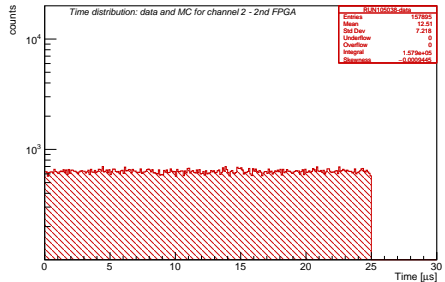
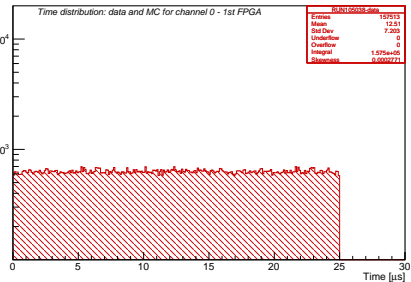
Hit timing distribution: overflow mode



- ▶ $T_{EW} = 50 \mu\text{s}$ and $f_{gen} = 60 \text{ kHz}$;
- ▶ The distribution of the hit time for channel 0 of digi-FPGA-1 (Left) and channel 2 of digi-FPGA-2 (Right);
- ▶ Different behaviour for different channels in different FPGAs: Left distribution is uniform, Right one is non-trivial;
- ▶ Apparently there are interruptions of channel 2 in the second FPGA;
- ▶ This behaviour can be explained with the *occupancy* plot.

Hit timing distribution: regular mode

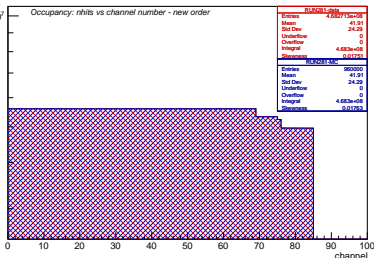
counts



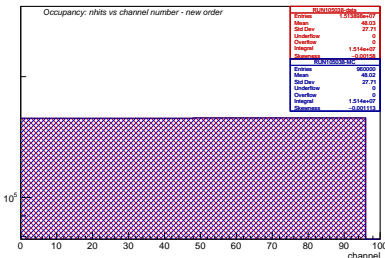
- ▶ $T_{EW} = 25 \mu\text{s}$ and $f_{gen} = 60 \text{ kHz}$;
- ▶ The distribution of the hit time for channel 0 of digi-FPGA-1 (Left) and channel 2 of digi-FPGA-2 (Right);
- ▶ Same behaviour for different channels in different FPGAs;
- ▶ No interruptions of channel 2 in the second FPGA.

Occupancy

counts

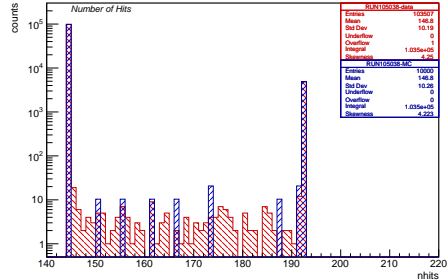
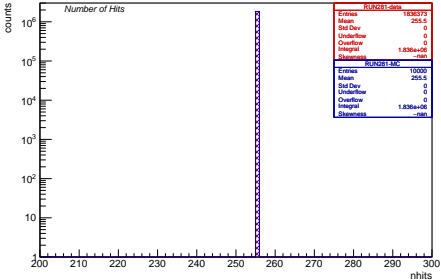


counts



- ▶ Occupancy plot: number of hits versus channel number (data red, MC blue);
- ▶ The bin ordering corresponds to the channel readout ordering;
- ▶ Overflow mode (Left):
 - channels 0-68: 48 digi-FPGA-1 channels with 4 hits (192 hits) and 21 digi-FPGA-2 channels with 3 hits (63 hits);
 - channels 0-75: 48 digi-FPGA-1 channels with 3 hits (144 hits) and 27 digi-FPGA-2 channels with 4 hits (108 hits) and 1 with 3 hits (111 hits);
 - channels 0-85: 48 digi-FPGA-1 channels with 3 hits (144 hits) and 37 digi-FPGA-2 channels with 3 hits (111 hits).
- ▶ Regular mode (Right): all channels with same occupancy.

Number of hits



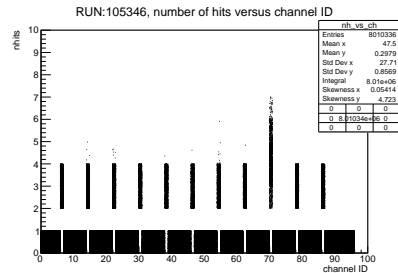
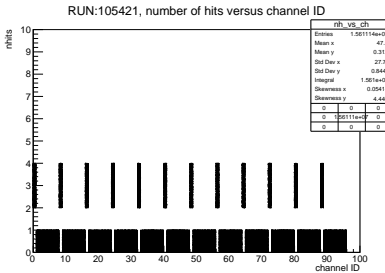
- ▶ Overflow mode (Left): distribution of number of hits peaked in 255;
- ▶ Regular mode (Right): the number of hits distribution depends on the relative offset of the EW with respect to the digi-FPGA pulsers and it varies from 144 to 192;
- ▶ Agreement between MC and data at a level of 10^{-3} .

Outline

- ▶ Commissioning of the tracker DAQ and FEE:
 - validation of ROC readout;
 - study of preamplifiers performance.
- ▶ First steps towards the station calibration;
- ▶ Pre-pattern recognition studies;
- ▶ Conclusions.

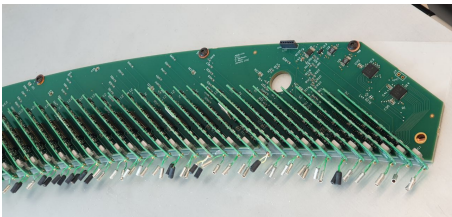
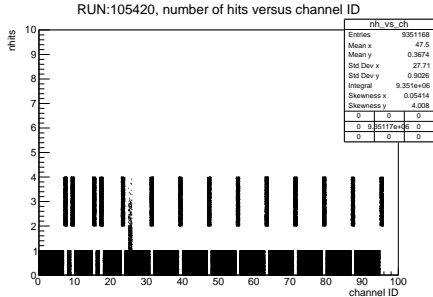
Test 1: channel occupancy

- ▶ Same test stand: 1 or 2 ROCs and one DTC + CAL side preamps;
- ▶ digi-FPGA generates calibration pulses (every 8th channel across 12 RUNs);
- ▶ Looking for cross talks, non-uniform occupancy, dead channels;
- ▶ The frequency was set to 50 kHz and $T_{EW} = 50 \mu\text{s}$, 2 or 3 hits per channel.



- ▶ (Left): regular occupancy;
- ▶ (Right): 94th channel dead (preamp substituted) and $N_{hits} > 3$ in some channels → waveforms shape study in Test 2.

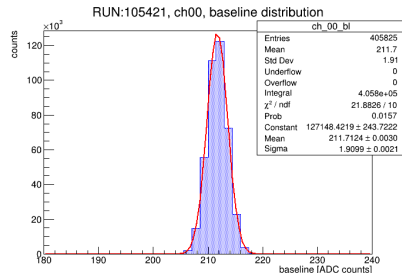
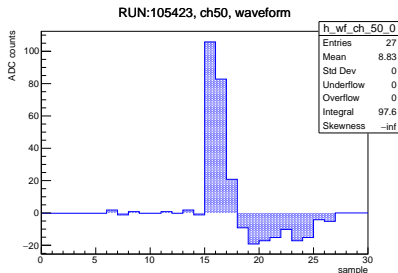
Test 1: channel occupancy



- ▶ (Left): occupancy plot with cross talks in first odd channels and only asymmetric (e.g. $3 \rightarrow 5$, not seen $3 \rightarrow 1$);
- ▶ (Right): preamp boards are mounted vertically and odd channels are those on the PCB board;
- ▶ The distance between the first channels is slightly lower;
- ▶ The solution to these cross talks is still object of study.

Test 2: analysis of readout waveforms shape

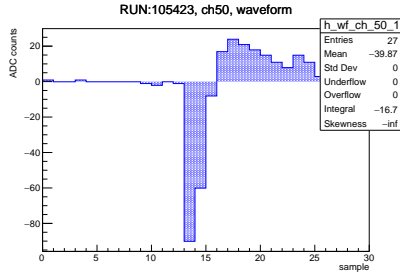
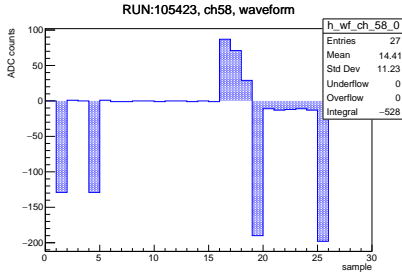
- ▶ Checking signal uniformity among channels within the same ROC or across multiple ROCs, and among different events;
- ▶ 40 MHz ADC (25 ns sample width) and pulser frequency set to 50 kHz.



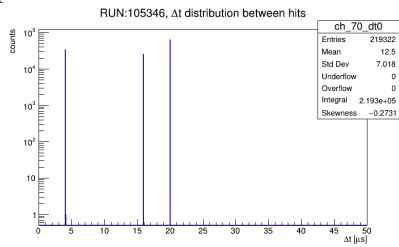
- ▶ (Left): regular waveform;
- ▶ Flat distribution in the first 10 samples (baseline), high positive charge peak with a sharp leading edge, negative tail;
- ▶ (Right): fitted baseline distribution, with mean at 210 ADC counts and $\text{FWHM} = 2\sqrt{2\ln 2}\sigma \sim 4.5$ ADC counts.

Test 2: analysis of readout waveforms shape

- Different baseline values indicating noise, dips, inverted waveforms.

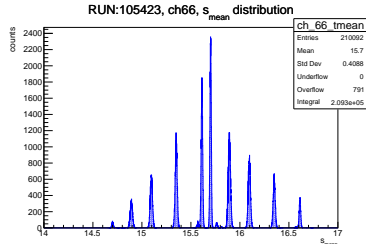
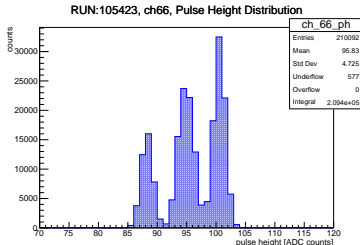


- (Left): dips of specific depths (64, 128 or 192) → ADC 6th or 7th bits;
- Problematic samples identified and excluded from the baseline estimate;
- (Right): inverted waveform → Δt distribution peaked in 16 μs (regular) and 4 μs (inverted). Trigger on trailing edge of 4 μs long input pulses.

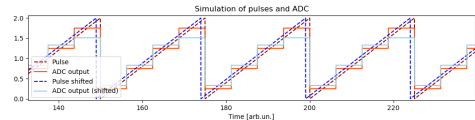


Test 2: analysis of readout waveforms shape

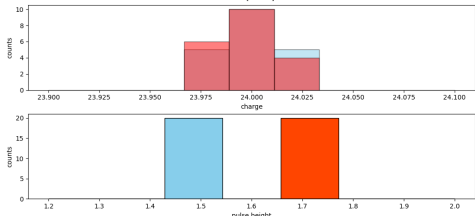
- (Left): pulse height (PH) (charge) distribution with 2/3 peaks.



- (Top Right): $s_{\text{mean}} = \frac{\sum_i \text{sample}_i \cdot q_i}{\sum_i q_i}$ distribution, correlated with PH (charge) peaks;

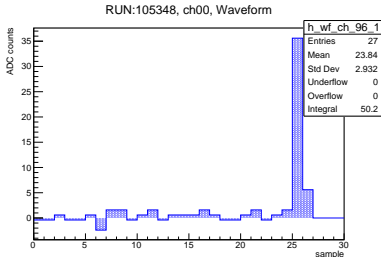
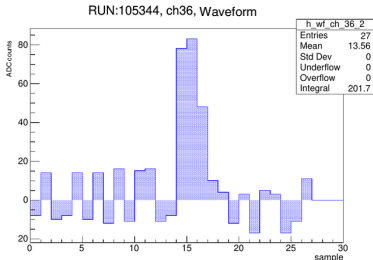


- (Bottom Right): simulation of the charge and PH distribution behaviour;
- This is an artifact of the pulser timing shifted with respect to the ADC clock of few ns.

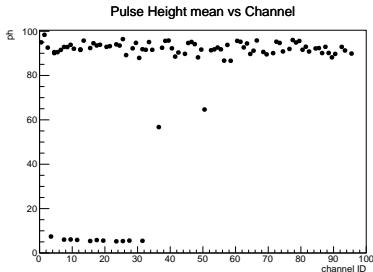
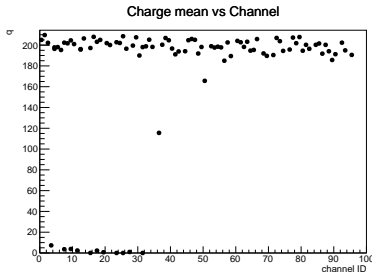


Test 2: analysis of readout waveforms shape

- ▶ Charge distribution used to check noisy channels (Left) and glitches (Right).



- ▶ Check of the response uniformity across channels.



Outline

- ▶ Commissioning of the tracker DAQ and FEE:
 - validation of ROC readout;
 - study of preamplifiers performance.
- ▶ First steps towards the station calibration;
- ▶ Pre-pattern recognition studies;
- ▶ Conclusions.

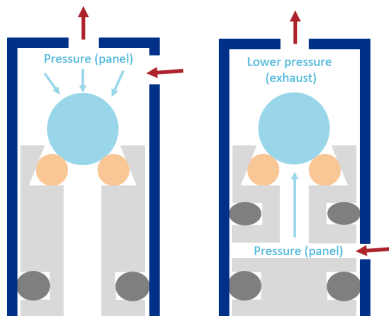
First steps towards the station calibration

- ▶ **Calibration goal:** straw longitudinal position resolution $\lesssim 4$ cm;
- ▶ TDCs measure arrival times t_1 and t_2 ;
- ▶ v : signal propagation velocity;
- ▶ x_{track} : reconstructed track on wire;
- ▶ **Calibration:** v from Δt_{12} (TDCs) correlated with x_{track} (**unbiased**);
- ▶ x_{track} determined by straw "yes or no" information \rightarrow **station geometry**.
- ▶ First calibration with **cosmics**;
- ▶ *Horizontal* \rightarrow unbiased reconstruction;
- ▶ **Operational constraints:** gas system, space, fragility. Designed to be operated **vertically**;
- ▶ **Simulation with vertical station to assess biases and feasibility.**

$$t_1 = t_0 + \frac{x_{\text{track}}}{v} + t_d + d_1$$

$$t_2 = t_0 + \frac{L - x_{\text{track}}}{v} + t_d + d_2$$

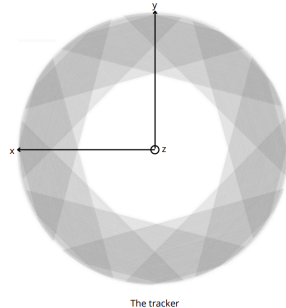
$$\Delta t_{12} = \frac{2x_{\text{track}} - L}{v} + (d_1 - d_2)$$



Monte Carlo muon selection and reconstruction

► Cosmics as calibration source:

- standard detector operations;
- flux is $\sim 1 \text{ cm}^{-2}\text{min}^{-1}$ (for horizontal detectors) and $E_{mean} \sim \text{GeV}$;
- MIP;
- $v_\mu \sim c \rightarrow$ align channel offsets.



► Straw information:

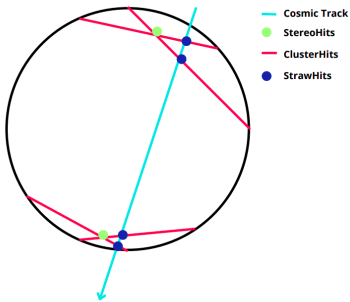
- the direction ($D_{x,i}, D_{y,i}$);
- the midpoint ($M_{x,i}, M_{y,i}$);
- the z_i coordinate.

► Selection:

- Hits in **one vertical station**;
- **Straight line in 3D**: ≥ 4 hits at different $z \rightarrow nhits_{face_i} \geq 1$;
- **Resolution**: $nhits_{panel_i} \leq 3$.

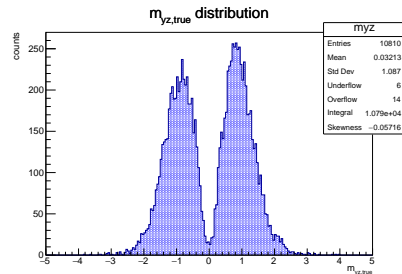
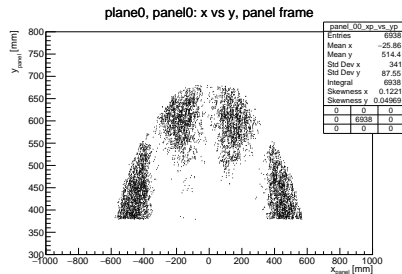
► Reconstruction:

- $StrawHits \rightarrow 1 ClusterHit$ (face);
- $2 ClusterHits \rightarrow StereoHit$ (plane);
- $2 StereoHits \rightarrow$ reconstructed track.



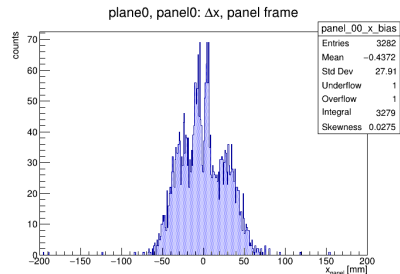
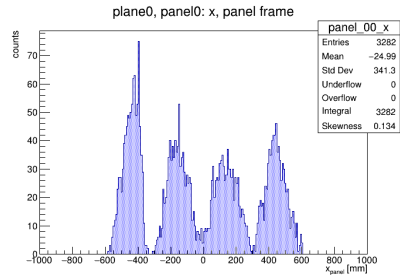
Panel illumination pattern and muon directions

- Precise calibration: uniformly distributed hits across the panel;
- (Top): muon selections bring to **non uniform** and spotty panel illumination;
- 4/4 overlap areas limited to **panel edges**;
- Time walk effects**;
- Selection of **specific muon directions**;
- (Bottom): $m_{yz} = \Delta y / \Delta z$ distribution;
- No particles with $m_{yz} \sim 0$ (horizontal) and $m_{yz} \rightarrow \infty$ (vertical);
- Mostly with $|m_{yz}| \sim 1$ (**45° angle**);
- Muon **rate** scaled by $1 / \cos^2 \theta \sim 1/2$ (45° flux) and $1/\sqrt{2}$ (cosmics striking at 45°).



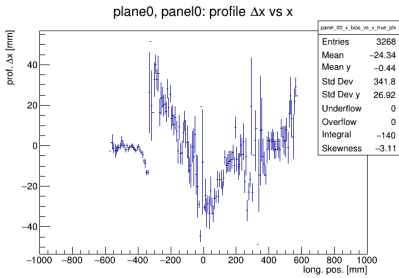
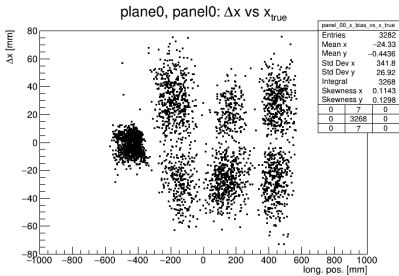
Longitudinal position reconstruction

- (Top): longitudinal reconstructed position x_{track} (panel frame);
- x_{track} : intersection of the reconstructed track with the mean z_i of the panel;
- **Bumps** \rightarrow 4/4 requirement consequence;
- Different bumps \rightarrow different straws;
- (Bottom): longitudinal reconstructed position **bias** (panel frame);
- $\Delta x = x_{track} - x_{true}$;
- x_{true} : MC panel hits mean coordinate;
- The bias ranges between [-6,6] cm;
- Similar distributions for all panels;
- Different straws with different bias;
- $m_{yz} = \frac{\Delta y}{\Delta z}$ not accurately reconstructed.



Results

- (Top): 2D distribution of Δx vs x_{true} ;
- Different spots → different overlap regions and muon directions;
- (Bottom): Δx profile vs x_{true} ;
- x_{track} reconstruction systematics ± 4 cm;
- $m_{yz} = \frac{\Delta y}{\Delta z}$ not accurately reconstructed;
- Vertical station: **opposite $y - z$ orientated muons do not cancel out**;
- First spots: 90° panels overlap;
- **Increase of data-taking time**;
- **This calibration is expected to become challenging.**



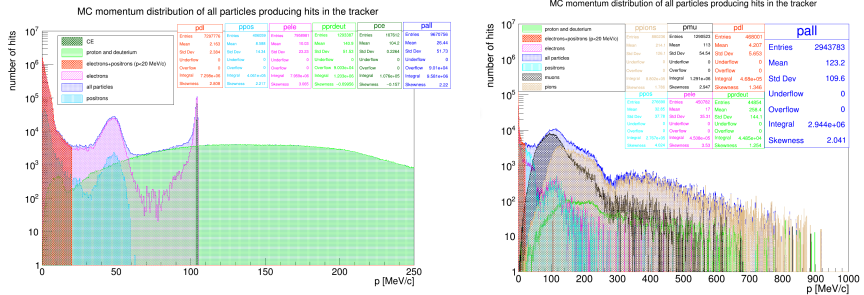
Outline

- ▶ Commissioning of the tracker DAQ and FEE:
 - validation of ROC readout;
 - study of preamplifiers performance.
- ▶ First steps towards the station calibration;
- ▶ Pre-pattern recognition studies;
- ▶ Conclusions.

Introduction

- ▶ Most of **tracker hits** are e^- and e^+ with $E < 20 \text{ MeV}$ - **δ -electrons**:
 - **Compton scattering**: interaction of γ s (n capture) with material;
 - **e^\pm pairs**: nuclear processes;
 - **δ -rays**: interaction of high-energy charged particles with material.
- ▶ Mu2e data: $\geq 7 \text{ PB/year} \rightarrow \text{CPU optimization critical}$;
- ▶ Hit flagging is a crucial step for several **physics reasons**:
 - **CE track reconstruction efficiency**;
 - **Protons**: complementary source to determine muon stopping rate;
 - **\bar{p} background**: correct background estimate.
- ▶ **Data-sample** for pre-pattern recognition studies:
 - **CE-1BB**: CE signal + pileup (1.6×10^7 protons/pulse);
 - **CE-2BB**: CE signal + pileup (3.9×10^7 protons/pulse);
 - **PBAR-0BB**: $\bar{p}s$ and no pileup.

δ -electrons in Mu2e tracker

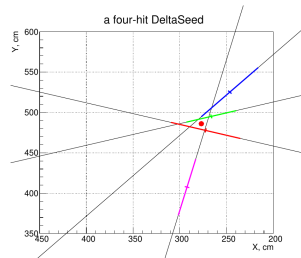
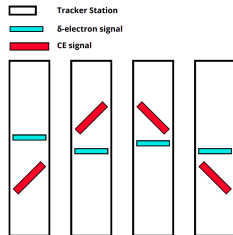


- Momentum distribution of particles making at least one hit in the tracker (Left: **CE-1BB**, Right: **PBAR-0BB**);
- (Left): 75% of hits by δ -electrons (71% e^- , 4% e^+ - Compton scattering);
- (Left): bump in the e^+ distribution ($N(\mu^+ \rightarrow e^+)/N(\mu^- \rightarrow e^-) \sim 10^{-3}$ for μ entering the DS and DIO on IPA should be also 10^{-3} wrt μ^- DIF);
- (Right): $p\bar{p}$ annihilation in ST \rightarrow multiple tracks with $p \sim 100/200$ MeV/c.

δ -electrons flagging algorithms

Two pre-pattern recognition algorithms developed in Mu2e Offline:

- ▶ **FlagBkgHits (FBH).** First it finds clusters of hits close in $x - y$ and time and uses an ANN to classify them. Based on *StereoHit* reconstruction.
Supervised training with CE+pileup dataset;
- ▶ **DeltaFinder (DF):**
 - δ segments in each station (*seeds*);
 - straws' center of gravity on $x-y$;
 - *seeds* across stations connected (δ candidate);
 - p candidates (*seeds* with $\bar{E}_{dep} > 3$ keV).



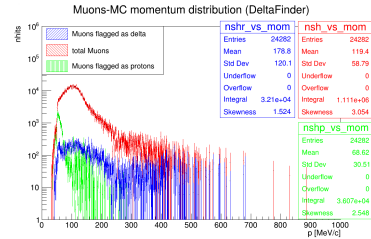
- ▶ (Left) δ -electrons and CE in the $r - z$ plane, (Right) δ candidate seed.

Performance analysis and comparison

Two levels of comparison:

- **hit-level:** how accurately individual hits are flagged (most direct method);
- **high-level:** reconstruction level comparison (figure of merit: CE tracks).
- Before comparing: **proton hit flagging over-efficiency by DF.**

	f_p	f_e
p	96.0%	1.0%
μ	5.8%	5.0%
π	2.5%	11.2%



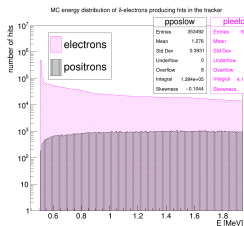
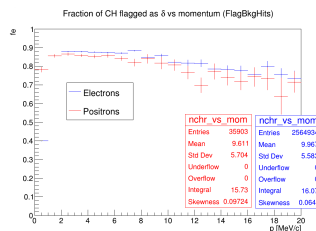
- (Left): f_p and $f_e \rightarrow$ fraction of hits flagged as p and e^- ;
- (Right): total (red) and flagged (green) μ hits vs the particle momentum;
- High μ and π $f_p \rightarrow$ low momentum (higher energy deposition as p);
- *Good* proton candidate $\rightarrow \geq 4$ hits with $E_{dep} > 3$ keV;
- ϵ_p reduced of 10%, but μ and π f_p reduced by factor of 2 and 6 \rightarrow next slide.

Hit-level comparison

- (Top Tab): **PBAR.** μ and π
 $f_{p,FBH}$ 4x and 3.3x higher;
- π : higher momenta;
- (Bottom Tab): **CE-1BB.**
 Same results for **CE-2BB** within 1%;
- **70% more CE hits flagged** as δ s by FBH wrt DF;
- **No p flagging comparison**
 (FBH identifies only high E_{dep} particles);
- (Left): e^- and e^+ f_e vs momentum (FBH);
- 1-2 MeV: Compton;
- >2 MeV: larger xy spread;
- (Right): e^- (pink) and e^+ (black) E distribution
 $(E < 2$ MeV).

	f_p DF	f_e FBH	f_e DF
μ	2.7%	13.0%	3.2%
π	0.4%	23.8%	7.3%

	f_p DF	f_e FBH	f_e DF
$e^- < 20$ MeV/c	2.5%	75.9%	72.5%
$e^- [20,80]$ MeV/c	1.0%	50.0%	27.4%
$e^- [80,110]$ MeV/c	0.3%	5.7%	3.4%
p	83.7%		1.0%
$e^+ < 20$ MeV/c	0.2%	85.5%	88.5%

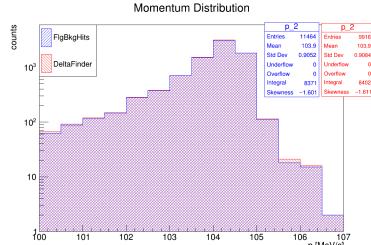
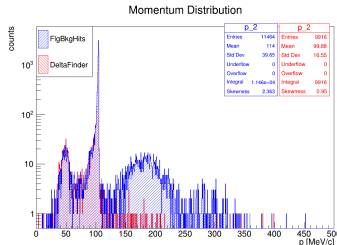


High-level comparison

- (Top Tab): **PBAR**. DF has 22% advantage in reconstructing 2 tracks (hit-level);
- 80 MeV/c cut: minimum reconstructable particle p from ST in the tracker;
- 90 MeV/c cut: DIO suppression;
- (Bottom Tab): **CE-1BB**. Same CE reconstruction efficiency (the hit-level difference is 1 hit/track);
- FBH (blue) & DF (red) reconstructed tracks p distributions (two ranges);
- FBH flags less proton hits and these hits are sent to pattern recognition.

fraction of events	FBH	DF
$N_{tracks} \geq 2$	1.8%	2.2%
$N_{tracks} \geq 2 \text{ & } p > 80 \text{ MeV/c}$	1.7%	2.1%
$N_{tracks} \geq 2 \text{ & } p > 90 \text{ MeV/c}$	1.6%	2.0%

	FBH	DF
CE events with $N_{tracks} > 0$	37.9%	37.9%



Outline

- ▶ Commissioning of the tracker DAQ and FEE:
 - validation of ROC readout;
 - study of preamplifiers performance.
- ▶ First steps towards the station calibration;
- ▶ Pre-pattern recognition studies;
- ▶ Conclusions.

Conclusions

- ▶ CLFV processes provide a clean test field for **NP models**;
- ▶ Mu2e is one of the leading experiments and searches for $\mu^- N \rightarrow e^- N$;
- ▶ Mu2e success depends on the performance of the **tracker**;
- ▶ **Comprehensive study** from the tracker readout to offline analysis:
 - DAQ and FEE testing:
 - ▶ **ROC readout validation** with MC at a level of 10^{-3} ;
 - ▶ **Preamps performance study**: dead channels, cross-talk between the channels, and waveform patterns study.
 - First steps towards timing calibration:
 - ▶ **Vertical station orientation** → non-uniform panel illumination;
 - ▶ Large **bias** on x_{track} reconstruction (± 4 cm);
 - ▶ Increase of data-taking time;
 - Pre-pattern recognition study to flag δ -electrons:
 - ▶ **Hit-level**: FBH flags 70% more CE hits, same performance for δ s, no possible p flag comparison, FBH not trained on \bar{p} data sample;
 - ▶ **High-level**: same reconstruction performance for CE signal;
 - ▶ **Timing**: 0.13, 0.39 ms/ev (1BB, 2BB) more for DF vs 5 ms/ev expected;
 - ▶ **Important to improve TimeCluster efficiency**.

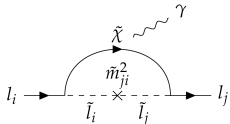
Thank you for your attention!

Bibliography

- [1] BERNSTEIN, R.H. AND COOPER, PETER S., *Charged lepton flavor violation: An experimenter's guide*, Physics Reports, 532 (2013), pp. 27–64.
- [2] BERNSTEIN, ROBERT H., *The Mu2e Experiment*, Frontiers in Physics, 7 (2019).
- [3] M. COLLABORATION, *Mu2e Run I Sensitivity Projections for the Neutrinoless $\mu^- \rightarrow e^-$ Conversion Search in Aluminum*, Universe, 9 (2023).
- [4] H. KOLANOSKI, N. WERMES, *Particle detectors*, Oxford University Press, 2020.
- [5] KARGIANTOULAKIS, MANOLIS, *A search for charged lepton flavor violation in the Mu2e experiment*, Modern Physics Letters A, 35 (2020), p. 2030007.
- [6] L. CABIBBI, G. SIGNORELLI, *Charged Lepton Flavour Violation: An Experimental and Theoretical Introduction*, La Rivista del Nuovo Cimento, 41 (2018), pp. 71–174.
- [7] MU2E COLLABORATION, *Mu2e Technical Design Report*, 2015.

BACKUP SLIDES

Beyond the SM



SUSY contribution to $l_i \rightarrow l_j \gamma$ via *slepton*

► Supersymmetry:

- particle with superpartner (different spin), lepton \rightarrow *slepton*;
- no common mass eigenstate base \rightarrow *slepton* superposition of flavours;
- CLFV suppression \rightarrow separation of the ν and W masses;
- SUSY breaking at electroweak scale ($\sim 10^2$ GeV) \rightarrow observable violation.

► Two Higgs Doublet model:

- two Higgs bosons;
- non-zero off-diagonal terms \rightarrow flavour violating Yukawa couplings

► Leptoquark models

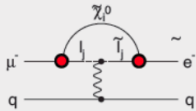
- LQ has both a baryon and lepton number.
- quark and lepton sectors are unified \rightarrow direct coupling via LQ exchange;
- specific CLFV processes are mediated by LQs.

► Additional Neutral Gauge Boson:

- Gauge boson mixes with SM neutral Gauge boson \rightarrow two mass eigenstates (Z , Z'). CLFV from off-diagonal terms in neutral current couplings to fermions.

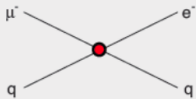
Supersymmetry

rate $\sim 10^{-15}$



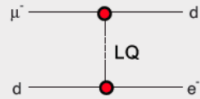
Compositeness

$\Lambda_c \sim 3000$ TeV



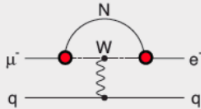
Leptoquark

$$M_{LQ} = 3000 (\lambda_{\mu d} \lambda_{ed})^{1/2} \text{ TeV}/c^2$$



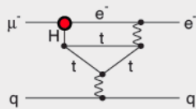
Heavy Neutrinos

$$|U_{\mu N} U_{e N}|^2 \sim 8 \times 10^{-13}$$



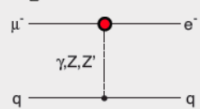
Second Higgs Doublet

$$g(H_{\mu e}) \sim 10^{-4} g(H_{\mu \mu})$$



Heavy Z' Anomalous Z Coupling

$$M_{Z'} = 3000 \text{ TeV}/c^2$$



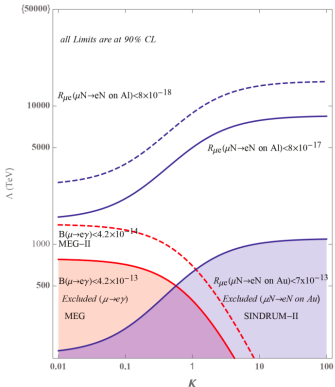
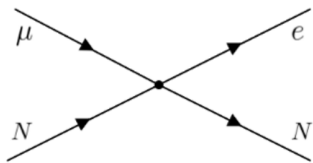
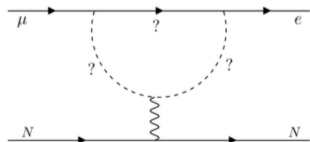
Muon channels

- ▶ μ s: most promising channel ($\mu^+ \rightarrow e^+\gamma$, $\mu^- N \rightarrow e^- N$ and $\mu^+ \rightarrow e^+e^+e^-$);
- ▶ μ production favored in π and K decays by hadronic interactions;
- ▶ Long lifetime \rightarrow muon beams;
- ▶ Small mass: limited number of decay modes available;
- ▶ $\mu^+ \rightarrow e^+\gamma$:
 - e^- and γ (52.8 MeV each and simultaneous);
 - positive muons \rightarrow no nuclear capture;
 - Radiative Muon Decay $\mu^+ \rightarrow e^+\nu_e\bar{\nu}_\mu\gamma$;
 - Accidental coincidence of $\mu^+ \rightarrow e^+\nu_e\bar{\nu}_\mu$ with a γ ;
 - Both backgrounds depend directly on $\Gamma_\mu \rightarrow$ continuous beam;
- ▶ $\mu^+ \rightarrow e^+e^-e^+$:
 - simultaneous 2 e^+ and 1 e^- with total energy equal to the M_μ ;
 - momentum range from few MeV to $M_\mu \rightarrow$ excellent tracker resolution;
 - Radiative Muon Decay $\mu^+ \rightarrow e^+\nu_e\bar{\nu}_\mu\gamma$ with internal conversion $\mu^+ \rightarrow e^+e^+e^-\nu_e\bar{\nu}_\mu$;
 - coincidence of one Michel decay with a e^+e^- pair (1-MD) or two Michel decays with a single e^- (2-MD);
 - continuous beam is preferred.

Charged Lepton Flavour Violation

- **EFT** Lagrangian parametrisation (model-independent): Λ is the effective mass scale and κ controls the relative contribution of the dipole moment term and the four fermion term.

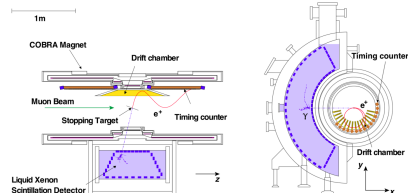
$$\mathcal{L}_{CLFV} = \frac{m_\mu}{(1 + \kappa)\Lambda^2} \bar{\mu}_R \sigma_{\mu\nu} e_L F^{\mu\nu} + \frac{\kappa}{(1 + \kappa)\Lambda^2} \bar{\mu}_L \gamma_\mu e_L \left(\sum_{q=u,d} \bar{q}_L \gamma^\mu \bar{q}_L \right)$$



$\mu^+ \rightarrow e^+ \gamma$ experiments

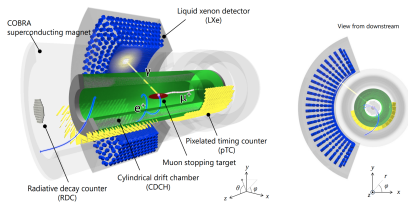
► MEG:

- anti-bottle B that decreases uniformly from centre, pushing particles away;
- LXe detector for e^+ and γ tracking;
- low energy e^+ discarded by placing detector far from magnet axis;
- polyethylene target to stop μ in the center of the magnet;
- drift chamber and timing counters to measure the p_{e^+} .



► MEG II:

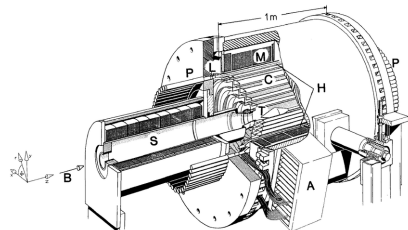
- to reduce the accidental background;
- muon flux increased ($7 \times 10^7 \mu^+/s$);
- thinner but more inclined ST;
- new cylindrical drift chamber (higher granularity and transparency);
- pixellated-TC;
- Radiative Decay Counter (low angle e^+).



$\mu^+ \rightarrow e^+e^-e^+$ experiments

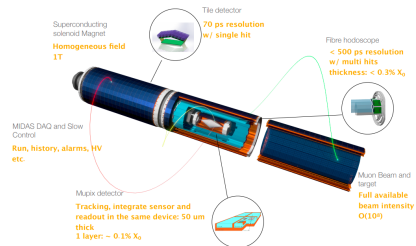
► SINDRUM I:

- double cone stopping target in the middle of five concentric multi-wire proportional chambers surrounded by plastic scintillator counters;
- solenoidal magnetic field;
- momentum resolution at the level of ~ 1 MeV, timing resolution ≤ 1 ns and a vertex resolution of ~ 1 cm.



► Mu3e:

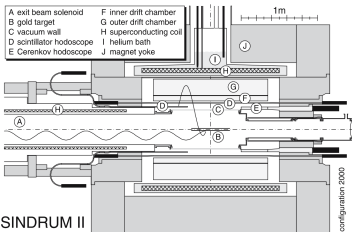
- goal of SES= 10^{-16} ;
- muons stopped on a thin hollow double-cone Mylar target;
- 2 m cylinder detector placed inside a 1.5 T magnetic field in 5 sections;
- central station: pixel detectors and scintillating fiber;
- 4 stations: pixel sensors and scintillator.



$\mu^- N \rightarrow e^- N$ experiments

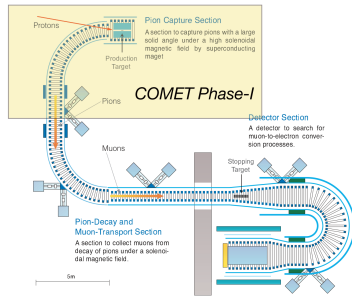
► SINDRUM II:

- cylindrical structure;
- target in the middle of the detector;
- drift chambers;
- CO₂-C₄H₁₀ and He-C₄H₁₀ trackers;
- plastic scintillators and Cherenkov;
- two hodoscopes at tracker ends;
- stopped μ : Ge(Li) detector.



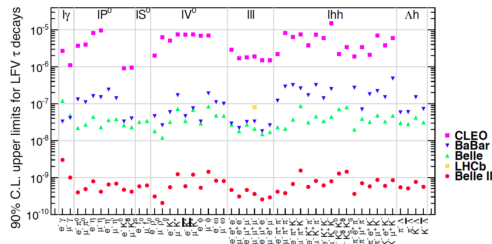
► COMET:

- C-shaped transport solenoid: tighter muon momentum selection, with a reduced beam intensity ($\sim 30\%$ less);
- additional curved solenoid after the stopping target (to remove e^-);
- Phase-I: understand experimental techniques and backgrounds;
- Phase-II: straw tube tracker and a LYSO EM calorimeter. Magnetic system expanded.



Tau channel

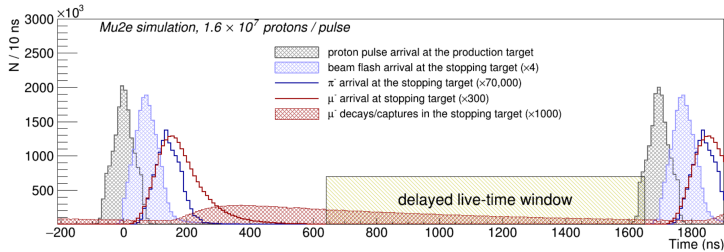
- ▶ τ : promising source of CLFV decays;
- ▶ Large mass ($m_\tau \sim 1.777$ GeV) \rightarrow multiple CLFV channels;
- ▶ $\tau \rightarrow l\gamma$ (radiative decay), $\tau \rightarrow 3l$ (three-body decay) and $\tau \rightarrow l h$;
- ▶ Higher predicted BR , wrt μs ($(\frac{m_\tau}{m_\mu})^\alpha$);
- ▶ No beams $\rightarrow \tau_\tau \sim 2.9 \times 10^{-13}$ s;
- ▶ Large detectors with good PID, tracking, calorimetry, hermeticity required;
- ▶ Low number of detectable τ s;
- ▶ $\tau^+ \tau^-$ produced by $\Upsilon(4s)$ resonance at $\sqrt{s} = 10.58$ GeV;
- ▶ Wide-range calibrations for detectors.



Reaction	Present limit	CL	Experiment	Year
$\mu^+ \rightarrow e^+ \gamma$	7.5×10^{-13}	90%	MEG II	2024
$\mu^+ \rightarrow e^+ e^+ e^-$	1.0×10^{-12}	90%	SINDRUM	1988
$\mu^- \text{ Ti} \rightarrow e^- \text{ Ti}$	6.1×10^{-13}	90%	SINDRUM II	1998
$\mu^- \text{ Au} \rightarrow e^- \text{ Au}$	7.0×10^{-13}	90%	SINDRUM II	2006
$\mu^+ e^- \rightarrow \mu^- e^+$	8.3×10^{-11}	90%	SINDRUM	1999
$\tau \rightarrow e \gamma$	3.3×10^{-8}	90%	BaBar	2010
$\tau \rightarrow \mu \gamma$	4.4×10^{-8}	90%	BaBar	2010
$\tau \rightarrow e e e$	2.7×10^{-8}	90%	Belle	2010
$\tau \rightarrow \mu \mu \mu$	2.1×10^{-8}	90%	Belle	2010

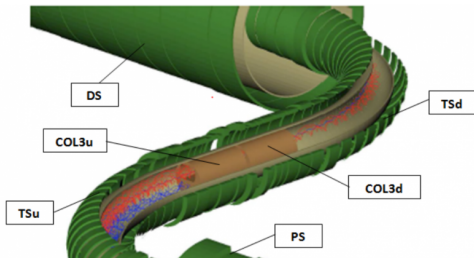
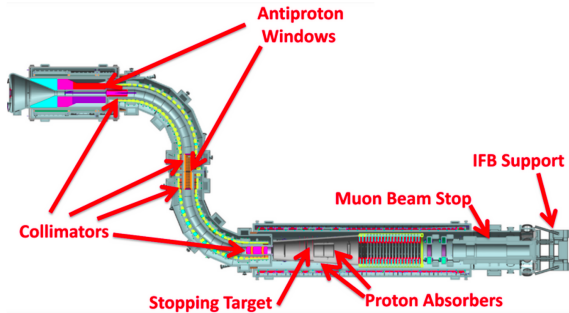
Table: Experimental upper limits for a variety of CLFV processes of leptons.

Pulsed proton beam



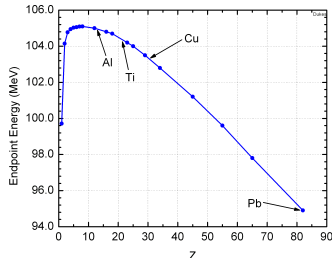
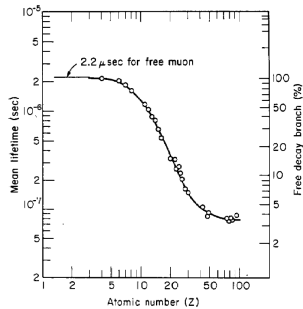
- ▶ 8 GeV, 8 kW beam originates from the Fermilab Booster;
- ▶ Proton pulses separated by 1695 ns and the delayed window is after 640 ns after the first pulse;
- ▶ Due to the short lifetime of pions, this background can be suppressed by using pulsed proton beam along with a delayed live-time window.

Mu2e beamline



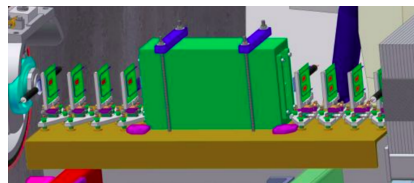
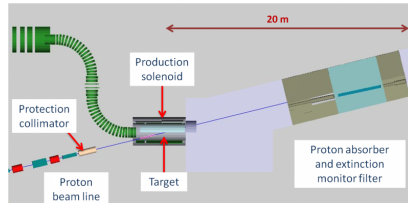
Why Al Stopping Target?

- ▶ Lower RMC background. Photon endpoint: $k_{max} = m_\mu c^2 - |E_b| - E_{rec} - \Delta M$ ~ 101.9 MeV, ~ 3.1 MeV below CE;
- ▶ (Top): quite long lifetime, allowing separation between prompt backgrounds and live window;
- ▶ (Bottom): DIO endpoint dependence on nucleus type. Al \rightarrow high endpoint. Higher- Z nuclei \rightarrow lower endpoint, minimizing background contribution;
- ▶ Conversion BR depends on the ST material. Comparison of conversion BRs on different nuclei normalized to aluminum \rightarrow dominating operator type. Materials with higher Z \rightarrow better model differentiation (Mu2e-II Ti);
- ▶ Available in required size/shape/thickness, low costs and chemically stable.



Extinction monitor

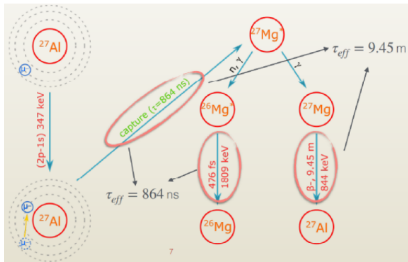
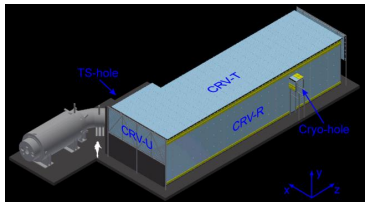
- ▶ Measures the fraction of out-of-time protons;
- ▶ Mu2e requirement: extinction $< 10^{-10}$;
- ▶ Two factors contribute to extinction: intrinsic accelerator extinction (2.1×10^{-5}), and AC resonant dipole sweepers;
- ▶ Mu2e AC dipoles: sweep away out-of-time protons into collimators (5×10^{-8}) (10% accuracy);
- ▶ Extinction Monitor (EM): collimator and magnetic filter system, pixel telescope, trigger scintillators;
- ▶ Magnetic filter transport of particles generated at the PT to the EM;
- ▶ The pixel telescope tracks the trajectory and momentum of particles (permanent magnet + 8 scintillators).



Cosmic Ray Veto and Stopping Target Monitor

Cosmic Ray Veto:

- ▶ **Active veto:** 4 layers of extruded plastic scintillation counters;
- ▶ **Passive shielding:** Al absorbers between each layer;
- ▶ $\epsilon_{CRV} = 99.9\%$;
- ▶ μ 's signature: 3/4 vetoed.

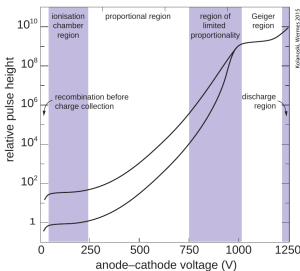
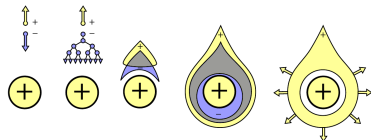
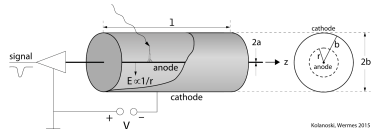


Stopping Target Monitor:

- ▶ HPGe and LaBr₃ detector → number of μ stopped in ST (10% precision on N_μ);
- ▶ It will measure the photons produced by secondary muonic aluminium orbital transitions (347 keV) and nuclear capture (884 keV, 1809 keV);
- ▶ Captured $\mu = 61\%$ of stopped μ .

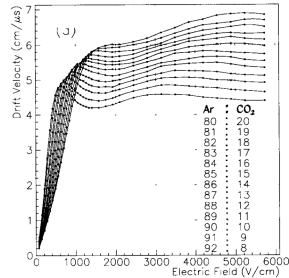
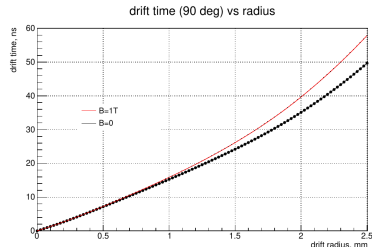
Drift tubes

- ▶ Cathode: grounded cylindrical conductor;
- ▶ Gases combination (noble, quench gas);
- ▶ Anode wire → high voltage $\mathcal{O}(\text{kV})$;
- ▶ $E(r) = \frac{1}{r} \frac{\lambda}{2\pi\epsilon} = \frac{1}{r} \frac{V}{\ln(b/a)}$ ($a < r < b$);
- ▶ Primary ionisation: $A C \rightarrow A^+ e^- C$, or $A C \rightarrow A^{++} e^- e^- C$;
- ▶ Excitation: $A C \rightarrow A^* C$;
- ▶ Secondary ionisation → avalanche;
- ▶ Induced signal dominated by ions movement;
- ▶ Proportional region;
- ▶ Quench gas (CO_2): needed to absorb photons from recombination and electron attachment and to prevent subsequent avalanches.



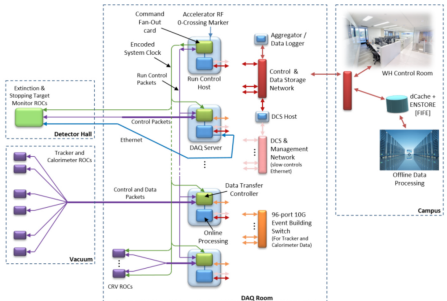
Drift tubes in magnetic field

- The sum of the electric drift field and magnetic field produce several effects:
 - change of the drift direction and velocity (v_d decreases as B increases);
 - reduction of diffusion transverse to the magnetic field.
- These effects depends on the type of drift gas and the magnetic and electric field relative orientation;
- $\vec{v}_D^B = -\frac{\mu^{B=0}}{1+\omega^2\tau^2} \left(\vec{E} + \frac{\vec{E} \times \vec{B}}{B} \omega \tau + \frac{(\vec{E} \cdot \vec{B}) \vec{B}}{B^2} \omega^2 \tau^2 \right)$;
- $\mu_B = 0$ mobility with zero magnetic field;
- $\omega = \frac{qB}{m}$ cyclotron frequency;
- τ electron average collision time in the gas;
- Mu2e straws orthogonal to B ;
- Angle between drift direction and B varies from 0° to 90° ;
- In Ar:CO₂, v_d depends on the electric field;
- Difference of 8 ns at radial distance of 2.5 mm.



DAQ system

- ▶ Streaming readout: digitized and zero-suppressed data;
- ▶ High data throughput, flexible for analysis;
- ▶ DAQ run control via RCH, managing a predefined Run Plan;
- ▶ Active spill defined by RF Zero-Crossing Markers from the Accelerator, synced to 1695 ns proton pulses, defining the EW;
- ▶ CFO module generates 40 MHz clock, embedding EWMs synced to the system;
- ▶ CFO distributes the clock and run control packets to DTCs in DAQ servers;
- ▶ DTCs pass the clock to ROCs and EWMs recovered;
- ▶ ROCs use EWMs to separate data from consecutive EWs;
- ▶ Data Requests trigger ROC data transmission through DTCs post-event;
- ▶ EBS routes data from multiple DTCs for online analysis;
- ▶ Events logged and transferred to long-term storage (7 PB/year);
- ▶ DTCs handle slow control data, managed by DCS Host and stored.

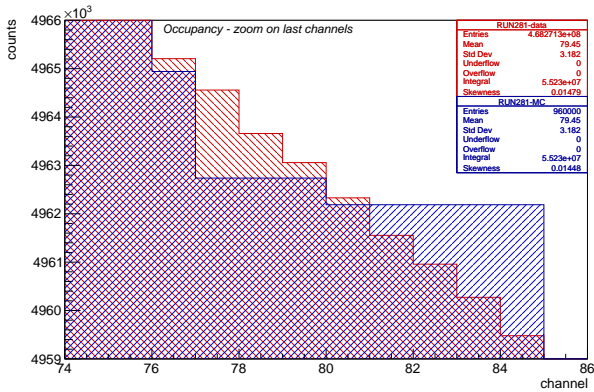


Tracker data format

A **hit data packet** has a fixed length of 256 bits (32 bytes). The packet structure is as follows:

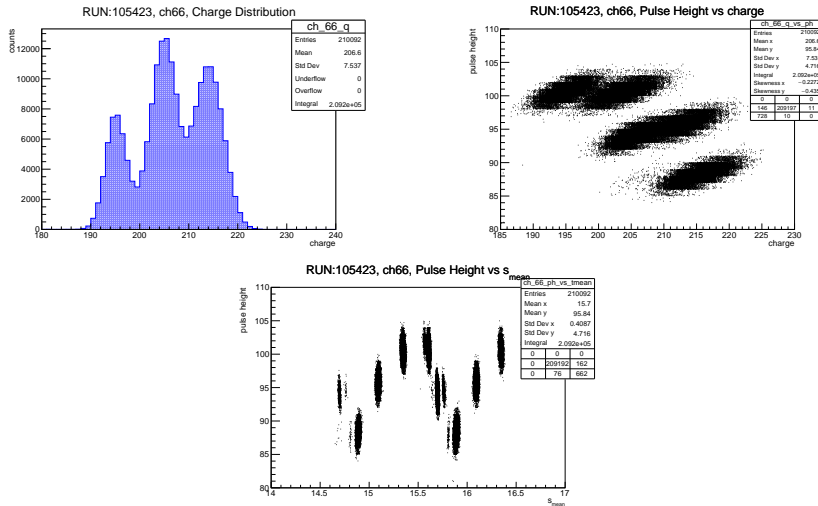
- ▶ 16 bit header (straw index);
- ▶ 16 bit for the TDC left straw end;
- ▶ 16 bit for the TDC right straw end;
- ▶ The ToT (time-over-threshold) values for the two ends of the straw are each stored using 8 bits;
- ▶ The ADC samples require 12 bits each. For each hit, a fixed number of samples (15) is readout;
- ▶ 12 bits are set aside for preprocessing flags.

Additional plots



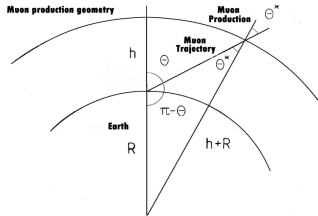
- Zoom on the last readout channels of the occupancy plot.

Additional plots



- ▶ (Left): The (positive) charge distribution of the waveforms (channel 66);
- ▶ (Right): 2D distribution of pulse height versus (positive) charge.

Cosmic muons simulation with CRY



- ▶ CRY (LANL) was used to generate cosmics (straightforward implementation);
- ▶ It simulates protons (1 GeV, 100 TeV), at the top of the atmosphere and generation of muons from the pion decays.
- ▶ It follows Gaisser-Tang model:

$$\frac{dI}{dE_\mu d\Omega dt dS} = \frac{0.14}{\text{cm}^2 \text{ s sr}} \left(\frac{E_\mu}{\text{GeV}} \left(1 + \frac{3.64 \text{ GeV}}{E_\mu (\cos \theta^*)^{1.29}} \right) \right)^{-2.7} \left[\frac{1}{1 + \frac{1.1 E_\mu \cos \theta^*}{115 \text{ GeV}}} + \frac{0.054}{1 + \frac{1.1 E_\mu \cos \theta^*}{850 \text{ GeV}}} \right];$$

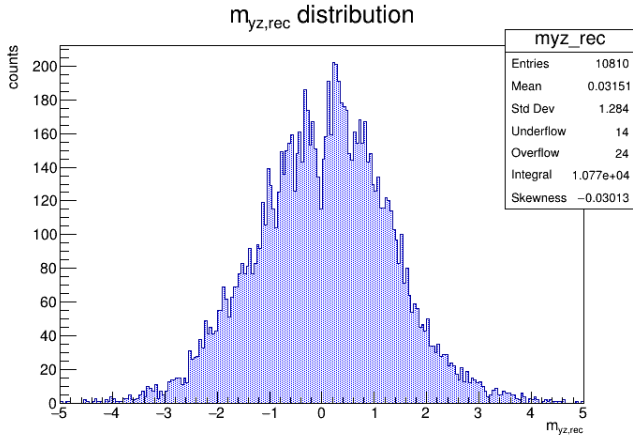
- ▶ $\cos \theta^*$ is given by: $\cos \theta^* = \sqrt{\frac{(\cos \theta)^2 + P_1^2 + P_2(\cos \theta)P_3 + P_4(\cos \theta)P_5}{1 + P_1^2 + P_2 + P_4}}$ with $P_1 \sim 0.10$, $P_2 \sim -0.07$, $P_3 \sim 0.96$, $P_4 \sim 0.04$ and $P_5 \sim 0.82$;
- ▶ (Top): θ^* and θ , zenith angle of muons and at the muon production point.

How to determine channel-to-channel delays

$$\frac{(t_1 + t_2)}{2} = t_d + t_0 + \frac{d_1 + d_2}{2} - \frac{L}{2v}$$

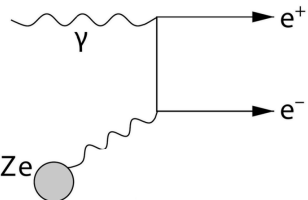
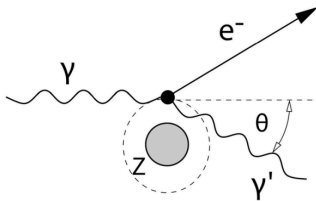
- ▶ $(t_1 + t_2)/2$ allows to measure the drift time up to an offset common to all channels.

Reconstructed muon direction



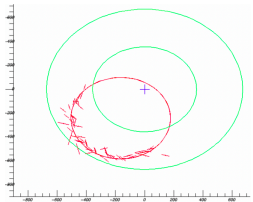
- ▶ Lots of muons reconstructed with $m_{yz} \sim 0$ (horizontal);
- ▶ The true hit position, far from the straws midpoint, results in incorrectly reconstructed tracks' direction on the $y - z$ plane.

δ -electron sources

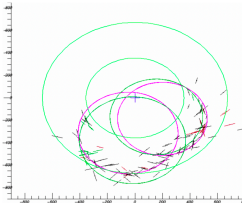


- **Compton scattering:** by γ s interacting with the detector material. Muon capture \rightarrow neutrons \rightarrow neutron capture γ emission ($E_\gamma \sim \text{MeV}$). The Compton effect (Left) is the scattering of a photon by a free or quasi-free ($E_\gamma \gg E_B$) electron. e^-/e^+ asymmetry. Compton cross section per atom proportional to Z ;
- **Pair production** (Right): from nuclear recoil processes. In the Coulomb field of a charge, a photon can convert into an $e^- - e^+$ pair. Z^2 dependence. $E_\gamma \geq 2m_e c^2 + 2\frac{m_e^2}{m_{\text{nucleus}}}c^2$;
- **Delta rays** (or secondary ionization electrons): generated when high-energy charged particles collide with the detector material. A particle collides with shell e^- , resulting in significant energy transfers.

\bar{p} background in Mu2e



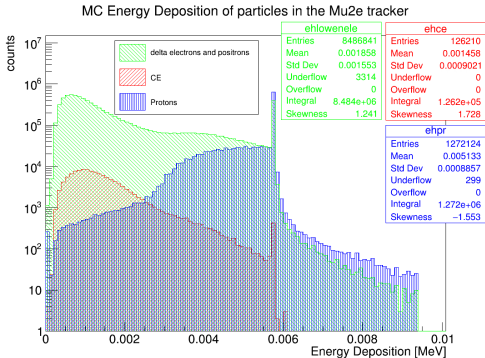
XY view



XY view

- ▶ $\bar{p}s$ are produced from pW interactions;
- ▶ $p\bar{p}$ annihilation at ST $\rightarrow e^-$ by $\pi^0 \rightarrow \gamma\gamma$ followed by γ conversions and $\pi^- \rightarrow \mu^- \bar{\nu}$;
- ▶ The background cannot be suppressed by cuts on the time window because $\bar{p}s$ are slower than other beam particles;
- ▶ There are absorber elements placed in the TS to suppress the $\bar{p}s$;
- ▶ $p\bar{p}$ annihilation at ST can give multiple particle tracks with $p \sim 100$ MeV/c for each track at much higher rate than signal-like;
- ▶ From MC, it was estimated that the rate of such multi-track events is $\times 500$ higher than the rate of events with 1 signal like e^- ;
- ▶ The analysis aims to reconstruct the multi-track final state events and get an estimate of the CE like events by rescaling the two final states ratio.

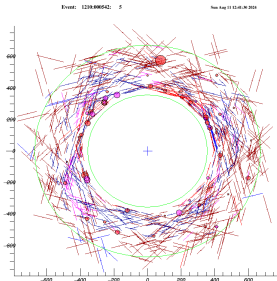
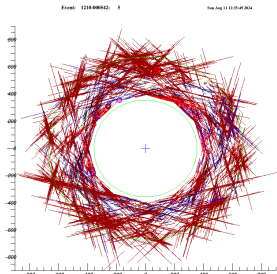
Monte Carlo deposited energy in the tracker



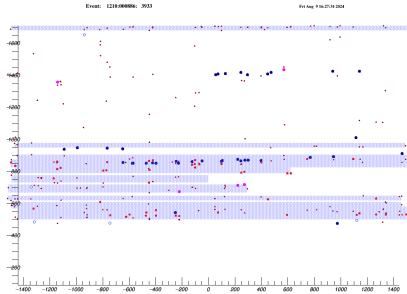
- The Monte Carlo deposited energy distribution in the tracker (*CE – 1BB* data sample);
- (Red) CEs, (green) δ -electrons, (blue) protons.
- Peaks and tails → saturated waveform;
- Only about 4% of CE hits have energies above 3.5 keV (1% above 5 keV);
- Applying an energy threshold in DF can speed up processing, but impacts algorithm efficiency, especially in *seed* reconstruction.

Mu2e event reconstruction

- ▶ Mu2e event reconstruction is optimised to reconstruct single-track events with tracks coming from the ST;
- ▶ Adjacent *StrawHits* within a panel, which are most likely due to the same particle, are combined into a *ComboHit*;
- ▶ δ -electron pre pattern recognition;
- ▶ We cluster the hits within a time window to form *TimeClusters* assuming that such hits are made by the same particle;
- ▶ Hits from *TimeClusters* are used to form helices;
- ▶ Final parameters of the track are determined by the Kalman fit.



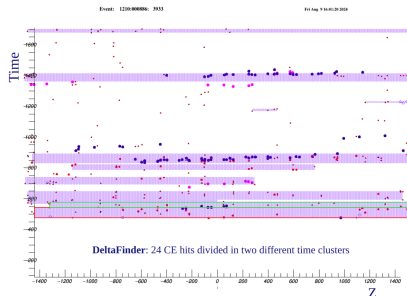
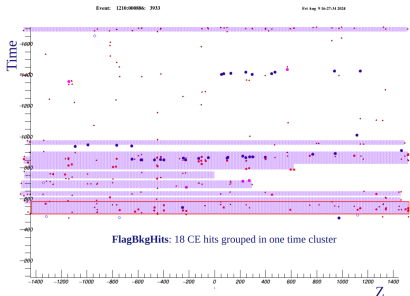
Time Clustering



Time clustering process:

- ① Combination of at least 3 *ComboHits* within a specific $time - z$ window (with a 20 ns time window and a 5-plane z-window);
- ② *Chunks* are created;
- ③ Every potential pair of chunks within a certain time proximity is tested together, and the pair, that minimizes the $\chi^2/ndof$ when the hits are fit to a linear line, is combined;
- ④ Procedure repeated until no further combinations yield a $\chi^2/ndof$ below a set threshold.

Time Clustering development



- ▶ There is a well defined class of events where the effects of hit flaggers get washed out in the reconstruction by the time clustering algorithm;
- ▶ Example:
 - DF: hits from one particle divided in two different time clusters;
 - FBH: not flagged particle hits are used by the time clusterer to *connect* particle hits that are used in the reconstruction. That is why the track is reconstructed in this case.
- ▶ Improving the cluster finder and the pattern recognition could increase the track reconstruction performance.